Assessment of the effects of residual stresses on fatigue life of real rough Surfaces in lubricated contact

Maasi F AL-Mayali[1,2]
[1]School of Engineering
Cardiff University, U.K
[2]College of Engineering
Al-Qadisiyah University, Iraq
al-mayalimf@cardiff.ac.uk

H. P. EVANS
School of Engineering
Cardiff University
Cardiff, U.K
EvansHP@cardiff.ac.uk

K. J. SHARIF
School of Engineering
Cardiff University
Cardiff, U.K
SharifK@cardiff.ac.uk

***Abstract*—This paper explores the possible effects of residual stress fields resulting from plastic deformation of real rough surface asperities on subsequent fatigue. A finite element model for the elastic-plastic contact of rough surfaces using profiles taken from the surfaces of unrun test disks is used to obtain the residual stress fields. These residual stresses are then added to the elastic stress distribution obtained from an elastohydrodynamic analysis to see the effects on fatigue damage and fatigue life at the scale of the surface roughness asperities. For the current paper, Micro-EHL simulations were carried out using the modelling techniques described in detail in reference and a strain-life model was used for predicting multiaxial fatigue life. The results show the accumulated damage due to residual stress effects is concentrated near the surface of particular asperity features.**

Keywords— micropitting; surface fatigue; rough surface elastohydrodynamic lubrication; gears

I. INTRODUCTION

Micropitting *Fig. 1*, is considered a common fatigue failure phenomenon detected on the scale of roughness asperities of gears and other machine elements in rolling contact that are subject to cyclic loading [1]. The pits formed by micropitting are estimated to be between 10-30 μm in diameter and 5-10 μm in depth corresponding to the roughness asperity topography. Initial pitting is associated primarily with contacting process and can improve into sub-surface crack-branching [2]. Micro pitting is generally established in the dedendum surface of both the driving and the driven gears and in many situations extends to the pitch line zone. Damage also occurs in the addendum of teeth and shallow cracks are observed but to a lesser extent than for the dedendum [3]. It is believed that pitting of the surface asperities is attributable to local overstressing at the contact between the asperities of the teeth. These high concentrated values of stress may cause material at those high stress zone; and pitting propagation. If such pitting continuous to develop, it will ultimately result in failure of the gear elements and cause a significant loss of tooth profile accuracy. To accurately understand the contact mechanics of the surface micropitting phenomenon it is essential to find the detailed tooth loading in terms of asperity pressure, shear stress, and

Fig.1. Micropitting pattern on a helical wheel. (Errichello, 2012).

local subsurface stress under conditions of elastohydrodynamic lubrication (EHL) [4], which is considered the normal film creation mechanism in gear tooth contacts analysis. However, the local EHL mechanism may fail in the most severe cases of thin films/high roughness and transient direct solid interaction happens; this is known as the mixed lubrication regime where the tooth load is carried by a combination of fluid film pressure and boundary-lubricated asperity encounters. Different novel approaches have been made to solve the problem of mixed lubrication. Chang and Webster [5] investigated the effects of roughness profiles by modelling the rough surface with sinusoidal functions of small wavelength as compared to the contact area. This model takes into consideration the transient nature of the problem due to "moving roughness". Zhu and Ai [6] examined the problem of micro-EHL point contact with real three-dimensional surface roughness profiles. A full analysis for mixed lubrication in point contacts for the EHL problem was solved by partitioning the overall contact area into sub-areas of either solid contact or thin film separation [7]. A new approach for solving the EHL problem has been developed, where that the elasticity equation can be defined in terms of a differential form and that provides means for close coupling of the hydrodynamic and elastic deformation equations. This method has the advantage of keeping the film thickness and pressure variables simultaneously active and stable during the simulation process and that provides a significant reduction in the computation time [8]. The coupled differential deflection method was successfully used to model the micro-EHL transient problem in which the asperities were at least an order of magnitude greater than the minimum lubricant film thickness [9]. Holmes, Evans and Snidle [10]

Published in: Students on Applied Engineering (ICSAE), International Conference.
Date Added to IEEE Xplore: 09 January 2017.
DOI: 10.1109/ICSAE.2016.7810173.
Publisher: IEEE.
Conference Location: Newcastle upon Tyne, UK.

then developed unified solutions to predict transient asperity interactions for elliptical contacts and mixed lubrication problems. In the current paper, we report the application of these new numerical techniques to the analysis of micro-EHL in test rough gear surfaces used as part of a study of micropitting and fatigue damage accumulation calculations with and without including the residual stress due to running-in. The process of transferring the calculated residual stress field from the Abaqus FEA system to the EHL fatigue calculation will be examined critically and the best settings for interpolation from the non-structured Abaqus mesh to the structured EHL fatigue calculation mesh have been determined by careful evaluation and checking. Representative measured roughness profiles have been run against each other in a multi-profile mixed EHL analysis to determine the surface loading during passage through the contact area. The results of mixed EHL have been further processed to study the effects of including residual plastic stress on the fatigue history and the resulting predicted damage accumulation.

II. Modelling of Residual Stress of Real Asperities by Abaqus

This section describes the approach used for modelling elastic-plastic contact using the ABAQUS FEA software system. Representative surface profiles were selected from the experimental work for both unrun disks and a set of FEA contact analyses was carried out to select the best nominal loading for estimating the residual stress field associated with the level of asperity modification observed in experimental work. These residual stresses which developed in the material may have a significant effect on the fatigue life of the surfaces. The residual stress field was combined with the stress resulting from EHL analysis to give an improved indication of damage and to assess surface fatigue life. At the first stage of the contact simulation, the real unrun rough profile is superimposed on a smooth roller geometry with 38.1 mm radius to form a 2-dimensional deformable part that models the contacting part of the twin disk rig. Having taken unrun roughness profiles from the rig, 1.5 mm sections of the filtered unrun gear surface profile were imported to Abaqus using a Python script, to create the 2-dimensional deformable part. The final model contained four separate parts that represent the part of the disk to be analysed, which were assembled using an elastic-plastic model with strain hardening to create the rough roller part that was then loaded in plane strain against a rigid plane. This loads the rough roller part against a reflection of itself in the rigid counterface so that the profile asperities are aligned with their reflected counterparts. The residual stress field, residual profile shape and *x*,*y* coordinates of the nodes can be extracted from the FEA analysis corresponding to the specified load for further analysis to be carried out based on the results. The rough deformable body was subjected to a range of loads 500 MPa, 750 MPa, 1250MPa and 1500 MPa applied over the non-contacting surface of the roller part. These loads were then removed, bringing the two parts out of contact. The best nominal loading for estimating the residual stress field associated with the highly deformed asperity features was then selected as shown in *Fig. 2*.

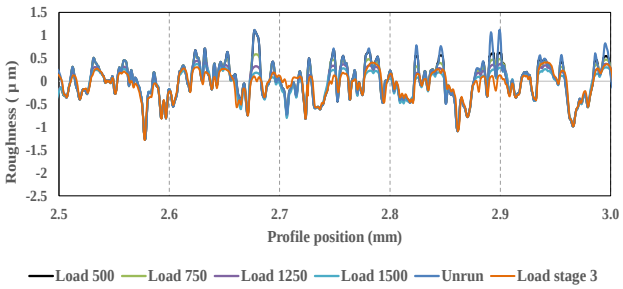

Fig.2. Representative section of surface residual profiles at a larger profile direction scale - the unit of the load is MPa.

III. Micro-Elastohydrodynamic Analyses

Evaluation of the fatigue model considered depends on the results of the transient micro-EHL solutions for fast and slow rough surface disks in rolling/sliding contact. Results of the micro-EHL modelling, which gives the full time-varying behaviour of lubricant pressure and film thickness, have been adopted in this paper to predict the fatigue life and accumulated damage at the scale of surface asperity features. The possible consequences on fatigue and damage of including the residual stress fields resulting from ABAQUS plastic deformation of the surfaces asperities were also investigated. The numerical analysis of real rough surface micro-EHL requires the simultaneous solution of the time dependent Reynolds equation and the elastic deflection equation. The novel methods that were used to solve the EHL problem, which defined by the fully-coupled, differential deflection approach, has been described by the authors in detail elsewhere [10], [11] and will not be repeated here. A typical profile sample with length 2.68 mm as shown in *Fig.3*, is selected for modelling of the rolling/sliding contact of the rough gear surfaces. This representative profile section was repeated and extended by creating longer multiprofiles with the joins between the repeated representative profiles effected at a mutual deep valley features in order to ensure no new artificial asperity features are established in the repeated profile. The purpose of using multiprofiles is to reproduce all the asperity interactions for the two surfaces during the of Micro-EHL contact simulation. The lubricant and other parameters assumed in the analyses are shown in Table 1.

The results of micro-EHL analyses are transient evaluations of lubricant pressure, surface shear stress and film thickness in the contact zone. The surface shear stress at direct asperity contact is calculated from the contact pressure using a boundary lubrication friction coefficient. The time-dependent pressure and shear stress results then used to predict the surface loading experienced by both contacting components. The output from micro-EHL simulations is therefore, most effectively presented as an animated series of lubricant pressure and film thickness profiles at the time steps used in the solution. The analysis output starts from the corresponding smooth surface steady state solution the roughness profiles gradually fed into the contact from the inlet boundary.

Published in: Students on Applied Engineering (ICSAE), International Conference.
Date Added to IEEE Xplore: 09 January 2017.
DOI: 10.1109/ICSAE.2016.7810173.
Publisher: IEEE.
Conference Location: Newcastle upon Tyne, UK.

TABLE 1 OPERATING CONDITIONS ASSUMED IN MICRO-EHL SIMULATION

Fast shaft speed (rpm)	200
Fast surface peripheral velocity(ms-1)	0.798
Slow surface peripheral velocity(ms-1)	0.479
Entrainment speed (ms-1)	0.638
Maximum Hertzian contact pressure (GPa)	1.4
Lubricant viscosity (Pas)	0.0257
Eyring shear stress (MPa)	10.0
Young's modulus (GPa)	207
Poisson's ratio	0.3
Hertzian contact dimension, a (mm)	0.469
Radius of surfaces 1 and 2 (mm)	38.1

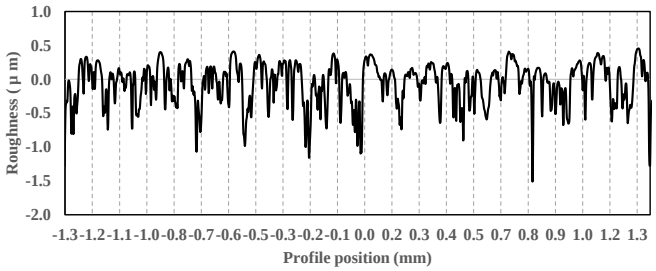

Fig.3. The representative profile section used in EHL simulations.

Every time step requires a converged solution of the pressure and film thickness with the current surface geometry. The lubricant pressure and film thickness values for the previous time step are used as starting values for the next time step during the solution process. An evaluation of the time-varying surface and subsurface elastic stress distribution may then be carried out for further analysis. *Fig.4*, shows the transient contact events happening during the micro-EHL analysis for the representative profile in a series of traverses of the contact zone.

Contact between asperities in the simulations were counted and accumulated relative to the surface roughness profile. In this way the number of time steps where contact occurred was obtained for each point in the profile. In this graph the results of five traverses are presented for the roughness profile. The roughness surface profile is shown as the lower of the curves in the figure with black colour. The five traverse count curves are offset from each other by a 'count' value of 100 for clarity and they are aligned with the representative roughness section. The total number of time steps required for a point on the rough profile to pass the Herzian contact width is 800, so a roughness profile location with a time step contact traverse count value of 100 corresponds to contact incidents occurring for 12.5% of the transit time. It is clear from these graph curves that the prominent asperities are seen to have high count values. Examples of this can be seen located at profile positions values of 274, 512 and 1164 µm having contact approximately between (8 – 12) % of the transit time in some of the traverses. For other traverses the contact counts at those profile location are relatively lower. *Fig.5*, illustrates the corresponding count of the number of time steps where maximum contact pressure values p > 3 GPa occurred. It is interesting to note that the same prominent asperities are seen to experience high count values in *Fig.5*, For example, those at profile position 73, 210, 367, 962 and 1240 µm. The variability between traverses

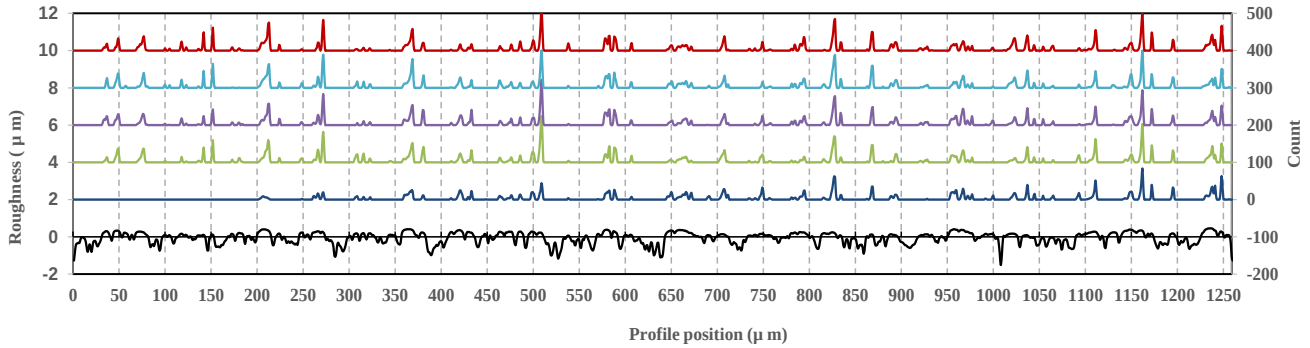

Fig.4. Profile contact count for five traverses of the contact zone.

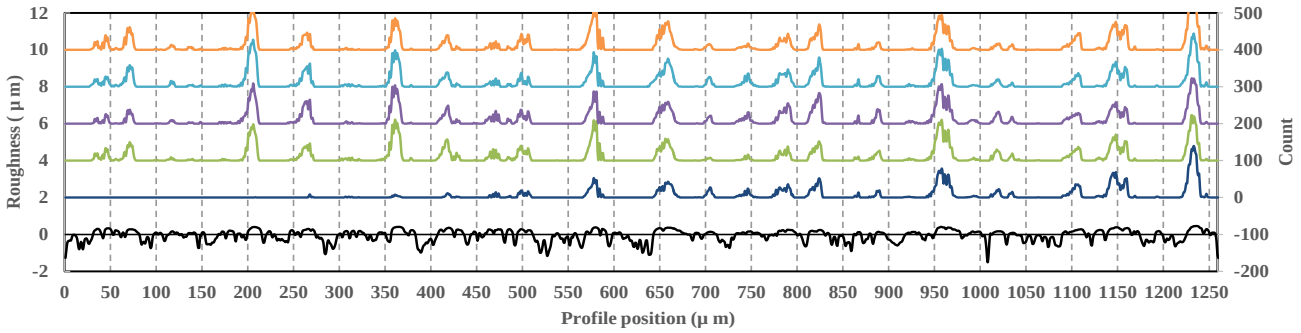

Fig.5. Profile high pressure count (p > 3GPa) for five traverses of the contact zone.

Published in: Students on Applied Engineering (ICSAE), International Conference.
Date Added to IEEE Xplore: 09 January 2017.
DOI: 10.1109/ICSAE.2016.7810173.
Publisher: IEEE.
Conference Location: Newcastle upon Tyne, UK.

results from the differences in the counterface asperities relative positions for each traverse. *Fig.6.* shows the pressure, film thickness distribution, in-contact cavitation and deflected smooth surface profiles for the smooth surface solution. The mesh size adopted in the micro-EHL simulations is $\Delta x = a/200$, where a is the Hertzian contact semi-dimension (a=0.469 mm). The equivalent smooth surface EHL solution has a maximum pressure of 1.5 GPa. *Fig.7,* shows the pressure, film thickness distribution and deflected rough surface profiles at a single time step during a transient simulations of two roughness profiles. The profiles are offset for clarity so that the relative magnitudes of the surface roughness asperities and the film thickness can be appreciated. The pressure, *p*, at micro asperity contacts is clearly seen to be much higher to the Hertzian semi-elllipse (2 to 4 GPa in many cases) and in this time step high extreme pressure spikes of 4, 3 and 3.25 GPa occur at positions x/a = -0.23, -0.8, 0.1, respectively, where the prominent surface asperity can be seen to be in close interaction. The black curve indicates the contact condition at each point in the mesh for the timestep. It has three levels correspanding to cavitated film(lower level), full film(central level) and direct contact(upper level). For the smooth surface result in Fig.6, only the full film and cavitated conditions occur with cavitation occurring at the exit to the Hertzian zone. In Fig.7, there are three occurences of direct asperity contact of x/a = -1, x/a = -0.8 and x/a = 0.3. The contact of x/a = -0.8 is associated with an extreme pressure but the others are not.

The outputs from transient analysis of two rough surfaces may prove to be important in terms of the sub-surface elastic stress, strain distributions calculations and fatigue damage estimation.The results are not considered until both surfaces have become rough from inlet to exit boundary. It is clear that an individual asperities will be subject to some cyclic loading as they pass through the contact zone thus incrasing the probability of the fatigue damage at the scale of the surface roughness.

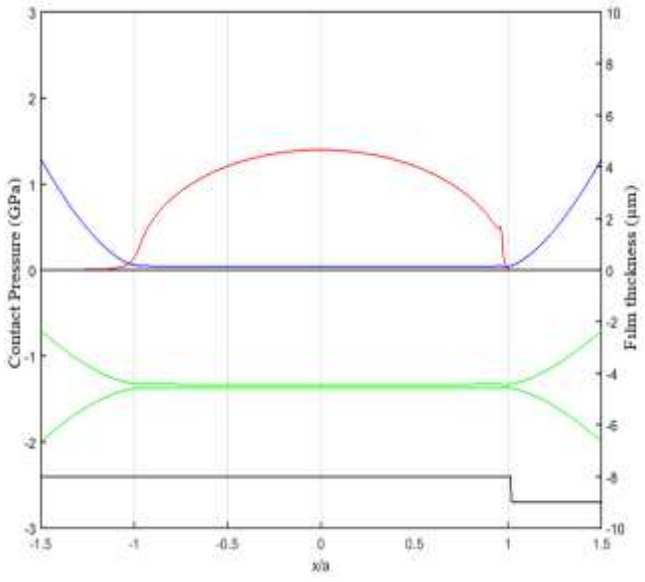

Fig.6. Pressure profile (red), film thickness distribution (blue) and deflected surface profiles (lower curves) at a smooth surface solution.

IV. Surface Fatigue and Damage Theory

The mixed EHL time step results are used to calculate the stress history at the lubricant/solid interface and for a block of the near surface material as it passes through the load bearing zone. The area of the block is chosen to be 2.6844 a parallel to the surface and a perpendicular to the surface. The block of material is subdivided with a rectangular element with mesh of 501x24 points. The stress history for the fixed points in the material as it passes through the EHL contact zone is crucial for assessing possible fatigue failure of the material and the microstructure changes. Thus, the fatigue damage calculated corresponds to one gear meshing cycle for the contacting material in the moving surfaces, or to one rolling contact cycle for the test disks used in the experiment. At every time step in the mixed EHL solution, the values of lubricant pressure, film thickness distribution and surface shear stress are obtained and used to calculate the instantaneous distribution of elastic stress history in the vulnerable thin surface layer. Equation (1) below has been used to calculate the instantaneous distribution of the sub-surface elastic stress.

$$\sigma(x, z, t) = \int_{x_1}^{x_2} p(s, t)F(x - s, z)ds + \int_{x_1}^{x_2} q(s, t)G(x - s, z)ds \qquad (1)$$

The symbols in Eq. (1) can be defined as: $\sigma(x,z,t)$ is the stress component, x is the tangential co-ordinate , z is the normal co-ordinate, t is time and F, G are the weighting functions for the stress component considered .
This assumes that the stress field stays in the elastic region and that any plastic behaviour has taken place with the run-in surface operating elastically following shakedown. These tress fields are used to compute the extent of fatigue damage employing cumulative damage criteria as described in [12]. The equivalent loading cycles at each point in the material are

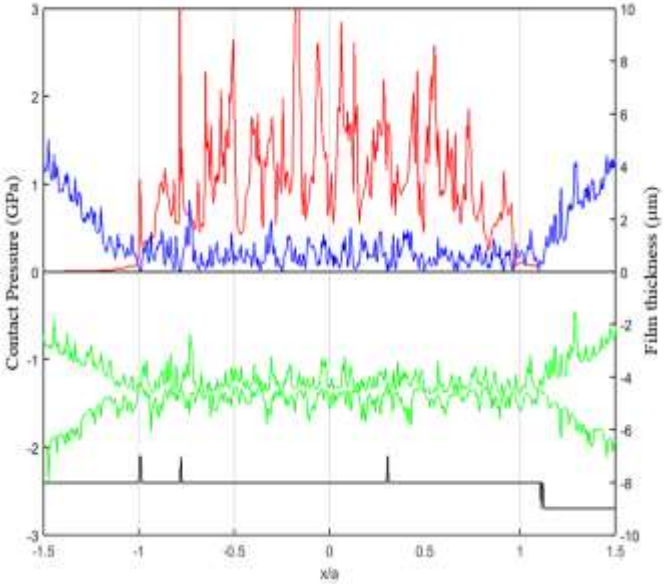

Fig.7. Illustrative a particular time step during the micro-EHL simulation: Pressure distribution (red curve), film thickness distribution (blue curve), in-contact cavitation (black curve) and deflected surface profiles (green curves).

Published in: Students on Applied Engineering (ICSAE), International Conference.
Date Added to IEEE Xplore: 09 January 2017.
DOI: 10.1109/ICSAE.2016.7810173.
Publisher: IEEE.
Conference Location: Newcastle upon Tyne, UK.

determined using the rainflow counting method [13]. For this paper the (shear) strain–life model proposed by Fatemi and Socie [14] has been used to calculate the number of repeated cycles that would result in fatigue, using equations of the form, as in (2) in critical plane analysis

$$\gamma_a \left(1+K\frac{\sigma_{n,max}}{\sigma_o'}\right) = \frac{\tau_f'}{G}(2N_f)^b + \gamma_f'(2N_f)^c \qquad (2)$$

In above (2) γ_a is the shear strain amplitude, $\sigma_{n,max}$ is the maximum tensile stress normal to plane during the effective loading cycle, N_f the number of loading cycles to failure and G is the Shear modulus. All orientation of the plan are considered and the critical plane is that for which the LHS of (2) is a maximum. Palmgren-Miner damage accumulation theory has been used to determine the accumulated damage for each effective loading cycle, as in (3), where D is the damage parameter. Fatigue will happen when a damage value becomes unity.

$$D = \sum_{\substack{\text{all effective} \\ \text{loading cycles}}} 1/N_f \qquad (3)$$

V. Results

Micro-EHL simulations were performed for both the fast and slow gears. In presenting and discussing results, we have focused only on the slow gear which suffers a greater level of calculated fatigue damage. *Fig.8,* shows the effect of different entrainment speed on the fatigue damage distribution. It is evident from this figure that the fatigue damage increases as the speed decreases, this is because of the reduction in lubricant film thickness in the contact area. It was found that for some asperities the fatigue life for the models involving residual stress was shorter than the fatigue life obtained using the same model without the induced residual stress as seen in *Fig.9*. Some of the experimentally observed micropits seen in

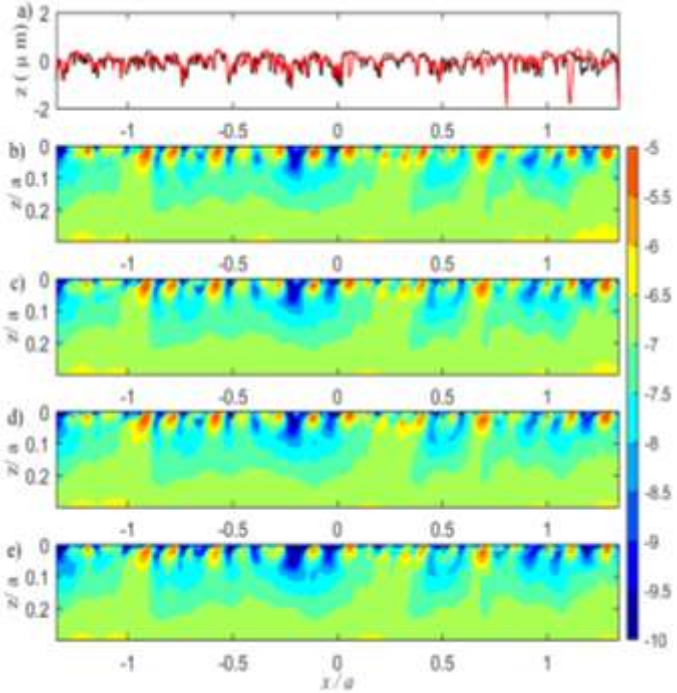

Fig.8. Contour of $\log_{10}(D)$ at different slow gear velocity: a) EHL profile; black is load stage 3; blue is load stage 18, b) 200 rpm, c) 500 rpm, d) 1000 rpm and e) 2000 rpm.

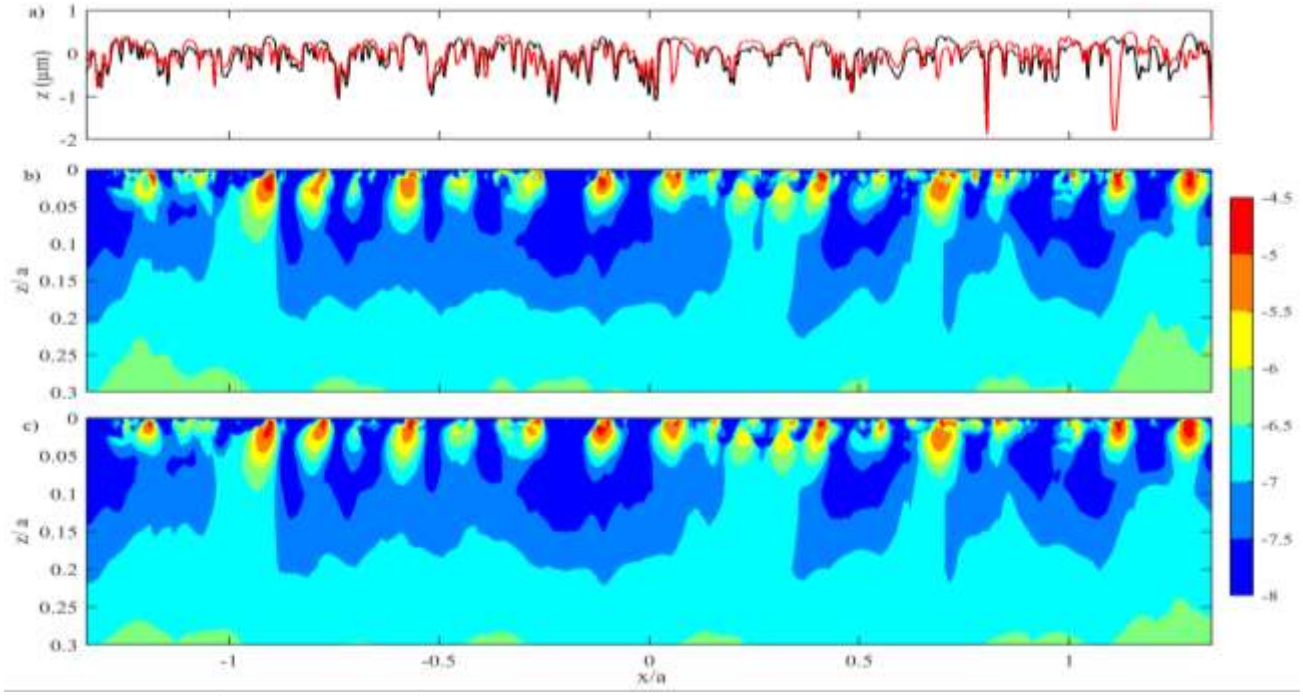

Fig.9. Contour of $\log_{10}(D)$: a) EHL profile, b) Damage with residual stress, c) Damage without residual stress.

Published in: Students on Applied Engineering (ICSAE), International Conference.
Date Added to IEEE Xplore: 09 January 2017.
DOI: 10.1109/ICSAE.2016.7810173.
Publisher: IEEE.
Conference Location: Newcastle upon Tyne, UK.

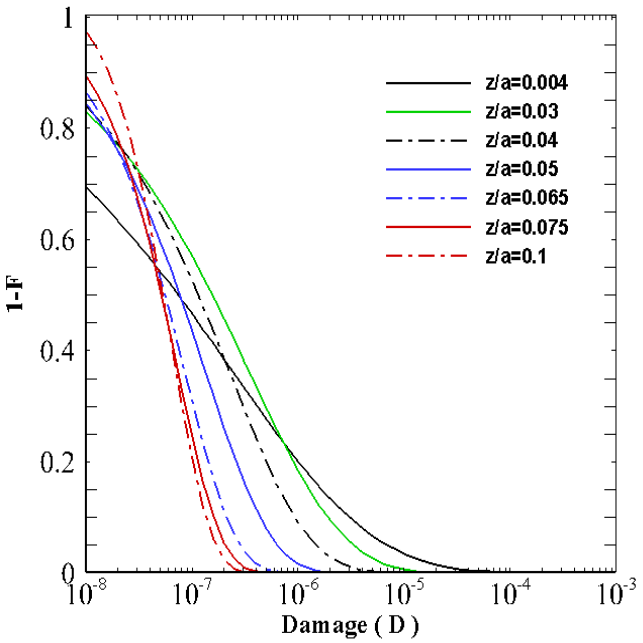

Fig.10. Cumulative damage distribution for the slower surface.

Fig.9, (a) were found to occur at positions that had high calculated fatigue damage. This shows that tensile residual stress can have a significant effect on the fatigue more detailed comparisons indicate that where this happens it tends to occur near the surface of the material. *Fig. 10*, above shows the Weibull distribution that describes the probability density function *f*(*D*) of damage at a different depth. The cumulative distribution indicates that the material would experience predicted fatigue failure in 10^7 gear meshing cycles.

VI. Discussion and Conclusion

The simulations of the gear tooth contacts show that contact pressures far in excess of the corresponding smooth Hertzian values that are created during a transient analysis due to surface roughness. Fatigue damage results show that the damage increases and moves to the sub-surface layer when roughness is present at a slower surface velocity. This is because these circumstances to higher asperity pressure in the mixed lubrication due to reduction of the entrainment effect. This supports the hypothesis that micropitting failure in gear teeth is mostly due to fatigue occurring at the level of the surface roughness asperities. Prominent asperities are subject to high damage risks because the damage value is effected by the asperity height and shape. The best settings for interpolation from the non-structured Abaqus mesh to the structured EHL fatigue calculation mesh have been determined by careful evaluation. Including residual stress due to plastic deformation in the fatigue analysis shows that most of the fatigue damage that is produced by residual stress is built up in the near surface layer. It was found that for some asperities including residual stress caused an increase in the calculated damage values.

VII. References

[1] M. Holmes, H. Qiao, H. Evans, and R. Snidle, “Surface contact and damage in micro-EHL,” Life Cycle Tribology Tribology and Interface Engineering Series, pp. 605–616, 2005.

[2] H. P. Evans, R. W. Snidle, K. J. Sharif, B. A. Shaw, and J. Zhang, “Analysis of Micro-Elastohydrodynamic Lubrication and Prediction of Surface Fatigue Damage in Micropitting Tests on Helical Gears,” J. Tribol. Journal of Tribology, vol. 135, no. 1, p. 011501, 2012.

[3] T. A. Stolarski and S. Tobe, Rolling contacts. London: Professional Engineering Pub., 2000.

[4] D. Dowson and G. Higginson, “Friction And Viscosity,” Elasto-Hydrodynamic Lubrication, pp. 161–181, 1977.

[5] L. Chang and M. N. Webster, “A Study of Elastohydrodynamic Lubrication of Rough Surfaces,” J. Tribol. Journal of Tribology, vol. 113, no. 1, p. 110, 1991.

[6] D. Zhu and X. Ai, “Point Contact EHL Based on Optically Measured Three-Dimensional Rough Surfaces,” J. Tribol. Journal of Tribology, vol. 119, no. 3, p. 375, 1997.

[7] X. Jiang, D. Y. Hua, H. S. Cheng, X. Ai, and S. C. Lee, “A Mixed Elastohydrodynamic Lubrication Model With Asperity Contact,” J. Tribol. Journal of Tribology, vol. 121, no. 3, p. 481, 1999.

[8] T. G. Hughes, C. D. Elcoate, and H. P. Evans, “Coupled solution of the elastohydrodynamic line contact problem using a differential deflection method,” Proceedings of the Institution of Mechanical Engineers, Part C: Journal of Mechanical Engineering Science, vol. 214, no. 4, pp. 585–598, Jan. 2000.

[9] C. D. Elcoate, H. P. Evans, T. G. Hughes, and R. W. Snidle, “Transient elastohydrodynamic analysis of rough surfaces using a novel coupled differential deflection method,” Proceedings of the Institution of Mechanical Engineers, Part J: Journal of Engineering Tribology, vol. 215, no. 4, pp. 319–337, Jan. 2001.

[10] M. J. A. Holmes, H. P. Evans, and R. W. Snidle, “Analysis of Mixed Lubrication Effects in Simulated Gear Tooth Contacts,” J. Tribol. Journal of Tribology, vol. 127, no. 1, p. 61, 2005.

[11] M. J. A. Holmes, H. P. Evans, T. G. Hughes, and R. W. Snidle, “Transient elastohydrodynamic point contact analysis using a new coupled differential deflection method Part 2: results,” Proceedings of the Institution of Mechanical Engineers, Part J: Journal of Engineering Tribology, vol. 217, no. 4, pp. 305–322, Jan. 2003.

[12] H. Qiao, H. P. Evans, and R. W. Snidle, “Comparison of fatigue model results for rough surface elastohydrodynamic lubrication,” Proceedings of the Institution of Mechanical Engineers, Part J: Journal of Engineering Tribology, vol. 222, no. 3, pp. 381–393, Jan. 2008.

[13] C. Amzallag, J. Gerey, J. Robert, and J. Bahuaud, “Standardization of the rainflow counting method for fatigue analysis,” International Journal of Fatigue, vol. 16, no. 4, pp. 287–293, 1994.

[14] A. Fatemi and D. F. Socie, “A Critical Plane Approach To Multiaxial Fatigue Damage Including Out-Of-Phase Loading,” Fatigue & Fracture of Engineering Materials and Structures Fat Frac Eng Mat Struct, vol. 11, no. 3, pp. 149–165, 1988.

Published in: Students on Applied Engineering (ICSAE), International Conference.
Date Added to IEEE Xplore: 09 January 2017.
DOI: 10.1109/ICSAE.2016.7810173.
Publisher: IEEE.
Conference Location: Newcastle upon Tyne, UK.